Supplementary Material

Materials and Methods

Experiment – The phase state of several binary mixtures of stars was investigated in squalene, a nearly athermal, non-volatile solvent. In most cases, experiments were conducted with 1,4-polybutadiene stars with a large star (with code 12880) having nominally $f_1 = 128$ arms[1]; its hydrodynamic radius was measured by dynamic light scattering in dilute solution and found to be[2] $R_{\rm h} = 51.4$ nm. Different small stars[3] were utilized with codes 36230, 14130 and respective hydrodynamic radii $R_{\rm h} = 40.2; {\rm nm}$ and $R_{\rm h} = 25$ nm; in the coding, the first three digits denote the functionality f_2 and the last two $M_{\rm w,arm}/(10^3$ g/mol). For all mixtures, the 12880 number density was fixed to $\rho_1\sigma_1^3 = 0.477$, where the effective corona diameter σ_1 coincides with the measured large-star hydrodynamic radius[2]; and the densities of the added small stars ranged from $\rho_2\sigma_1^3 = 0$ to $\rho_2\sigma_1^3 = 7.2$.

For one series of experiments we also used a mixture of stable star-like micelles in decane[4], an alternative to the micelles studied in Ref. 5. These micelles a based on arborescent polystyrene graft polyisoprene copolymers, where the polystyrene forms the core[4]. The particular mixture used consists of a large star with $f_1 = 170$, total arm molar mass $M_{\rm w,arm} = 29000$ g/mol and $R_h = 34.7$ nm and of a small star with $f_2 = 150$, total arm molar mass $M_{\rm w,arm} = 2900$ g/mol and $R_h = 11.4$ nm. The properties of the samples are summarized in Table SI.

Code	Functionality	$M_{\rm w,arm}$ [g/mol]	$p_{\rm arm}$	$p_{\rm star}$
12880	128	80000	1.04	1.02
36230	362	30000	1.06	1.14
14130	141	30000	1.08	1.03
17029	170	29000	1.06	1.27
15003	150	2900	1.04	1.07

TABLE SI: Properties of the studied samples. We list the coding, functionality, molar mass ($M_{\rm w}$), and star-arm polydispersity ($p_{\rm arm}$) and star polydipersity index ($p_{\rm star}$). The latter are the ratio of the weight-average and number-average molar mass.

The state of a given sample was investigated with linear rheological measurements; these were carried out with a sensitive strain-controlled rheometer (TA Instruments ARES-HR 100FRTN1). All measurements were performed in a cone-and-plate geometry ($25\,\mathrm{mm}$ diameter, $0.04\,\mathrm{rad}$ cone angle), except for samples with the highest concentrations for the mixture 12880/14130, which were measured in a parallel plate ($8\,\mathrm{mm}$ diameter) fixture. The temperature was set at $20 \pm 0.1\,^{\circ}\mathrm{C}$ with a recirculating water/ethylene glycol mixture. Where necessary (decane solvent) a home-made solvent trap system was used to reduce the risk of evaporation.

Special care was taken to account for the aging of the glassy samples, which typically was observed in the range of 0.5 to 1 day. In one particular case, the mixture 12880/14130 was observed to age for about 1 week. When conditions for reproducible and time-independent measurements were established, small strain amplitude oscillatory shear tests were carried out in the frequency range 100 to 0.01 rad/s. Analysis of the data provided information on the state of the sample studied and, in the case of solid-like behavior, the plateau modulus G'. Typically, a glassy state was characterized by a nearly frequency-independent storage modulus G' that exceeded the loss modulus G'' over a wide frequency range[2,6].

Theory and simulations – The theoretical investigations are based on a coarse-grained view of the stars with different functionalities, f_1 and f_2, which employs the effective interaction potentials derived in Ref. 7. We consider mixtures of large and small stars with several combinations of f_1 and f_2, with σ_i, $i = 1, 2$ denoting the corona diameters of the two stars. The size ratio δ is defined as $\delta \equiv \sigma_2/\sigma_1$. In the theoretical calculations, the number density of the large stars ρ_1 is kept constant at a value corresponding to a glassy state within Mode Coupling Theory[8]. The actual values of f_1, f_2, ρ_1 are reported in the figure captions. We study the dynamics of the mixture using two component MCT[9,10] . The required partial structure factors for MCT are calculated by solving the binary Ornstein-Zernike equation[11] with the Rogers-Young closure[12]. Within MCT, we have also calculated the the zero-frequency storage modulus[13] G', which is compared to the experimental results.

We also performed standard molecular dynamic simulations for a binary mixture of particles interacting with the above mentioned potential[7]. To be able to reach state points that are sufficiently close to the glass transition, and hence to suppress crystallization, a size polydispersity of 10% for the large stars only has been used in all simulations with $\rho_1\sigma_1^3 > 0.345$. We have studied a number of large particles varying between 250 and 2000 and a number of small particles ranging from 0 to 5000. The mass ratio between the large and small particles is assumed to scale as $\delta^{5/3}(f_2/f_1)^{1/3}$,

as discussed in Ref. 14. Time is measured in unit of $\tau_{MD} = \sqrt{k_B T/(m_1 \sigma_1^2)}$.

Two large stars closer than the distance corresponding to the first minimum in $g_{11}(r)$ are considered nearest neighbors. The symbol N_{11} is defined as the associated average number of large star neighbors. The inertia tensor I of a number n of point particles of unit mass with respect to their center of mass is defined as[15]:

$$I = \sum_{i=1}^{n} [\mathbf{r}_i^2 \mathcal{E} - \mathbf{r}_i \otimes \mathbf{r}_i], \tag{1}$$

where $\mathbf{r}_i$ is the coordinate of the ith particle with respect to the center of mass, $\mathcal{E}$ is the 3×3 identity matrix, and $\otimes$ denotes the dyadic product. We calculate the inertia tensor for the nearest neighbor cage of each large star, formed by the neighboring large ones. After that, we diagonalize it obtaining the eigenvalues $\lambda_1 \leq \lambda_2 \leq \lambda_3$. A robust measure of the cage anisotropy is given by the k_2-parameter, defined as

$$k_2 = 1 - \frac{27A}{B^3}, \tag{2}$$

with A and B being rotational invariants, defined as

$$A = \langle \lambda_1 \rangle \langle \lambda_2 \rangle \langle \lambda_3 \rangle ; \tag{3}$$

$$B = \langle \lambda_1 \rangle + \langle \lambda_2 \rangle + \langle \lambda_3 \rangle , \tag{4}$$

where the averages are taken over all large particles and several independent configurations.

Additional Results

- *MSD for different combinations of f_1 and f_2*

  Fig. S1 confirms that the dynamics of the large stars, as probed by numerical simulations, shows a reentrant behavior. The two sets of parameters are here chosen to be identical to the experimental values and to the MCT case reported in Fig. 1(c) and Fig. 1(d).

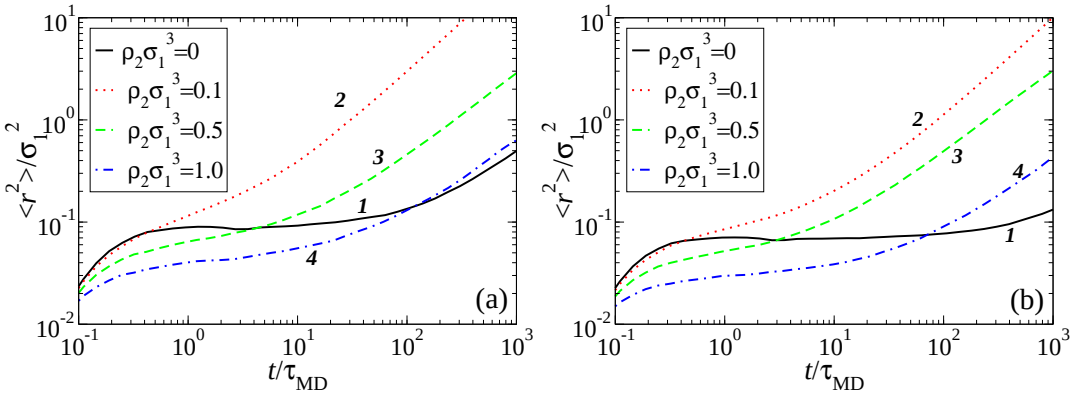

FIG. S1: Mean squared displacements of the large stars at $\delta = 0.4$ and increasing ρ_2. (a) Mixture with $f_1 = 128$ and $f_2 = 141$ at $\rho_1\sigma_1^3 = 0.39$; (b) $f_1 = 170$ and $f_2 = 150$ at the same ρ_1 as (a). In both cases the non-monotonic behavior as a function of additive density is evident. The lines are numbered in order of increasing additive density.

- *Partial radial distribution functions $g_{12}(r)$*

  Fig. S2 shows the results for the cross-correlation function $g_{12}(r)$ for the same state points discussed in Fig. 4 of the article. The correlations between the different species confirm that on increasing ρ_2, small stars penetrate deeper into the large-star cages. As a result, the height of the correlation peak grows. Note also that subsequent peaks are formed at distances compatible with sequences of small and large stars.

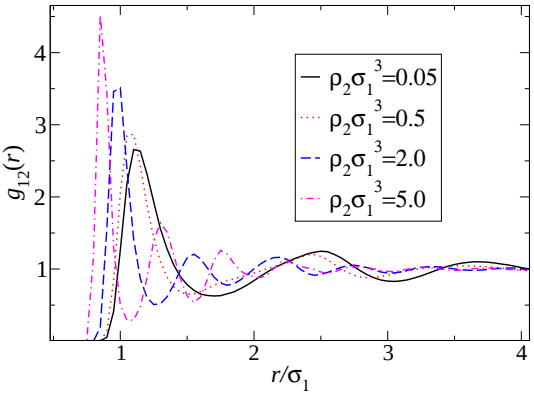

FIG. S2: Cross correlation function of the large and small stars $g_{12}(r)$ for $\rho_1\sigma_1^3 = 0.345$, $\delta = 0.4$ and increasing ρ_2. The peak moves to smaller distances, at the same time layering with a length scale $\sim \sigma_2$ appears.

- *Effect of δ on the radial distribution functions $g_{11}(r)$*

  Fig. S3 shows that the development of the structure on increasing ρ_2 at small δ is clearly different from the one observed for $\delta = 0.4$, shown in Fig. 4(a) and discussed in the manuscript. While the behavior for $\delta = 0.1$ can be interpreted in an effective depletion picture analogous to colloid-polymer mixtures, the behavior for $\delta \sim 0.4$ is clearly different: only a full, two-component MCT yields the double glass and the asymmetric glass, whereas an effective, one-component MCT yields simply a monotonically falling melting curve on the (ρ_2, δ)-plane[2].

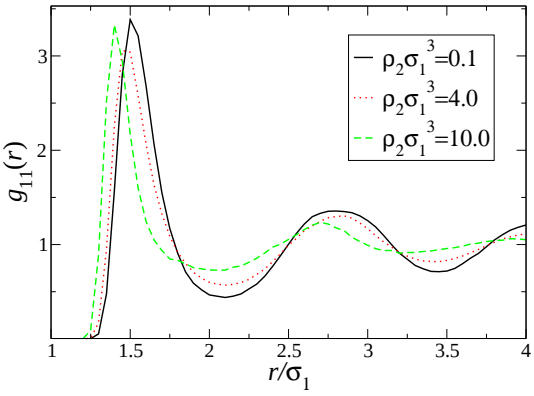

FIG. S3: Radial distribution function of the large stars $g_{11}(r)$ for $\rho_1\sigma_1^3 = 0.345$, $\delta = 0.1$ and increasing ρ_2. The shift of the peak position is much less pronounced than for larger δ. More importantly, no additional layering at the length scale of the small ones occurs.

- *Eigenvalues of the inertia tensor*

  To complement results reported in Fig. 4 of the manuscript, we show here the ρ_2 dependence of the normalized eigenvalues $\langle\lambda_i\rangle/N_{11}$, $i = 1, 2, 3$. They decrease monotonically on increasing the additive concentration. Moreover, the ratios $\langle\lambda_1\rangle/\langle\lambda_3\rangle$ and $\langle\lambda_2\rangle/\langle\lambda_3\rangle$, shown in Fig. S4, display a significant reduction, signaling the growing anisotropy of the cages. It can be clearly seen than one of the eigenvalues decouples from the other two, signaling an increasing anisotropy.

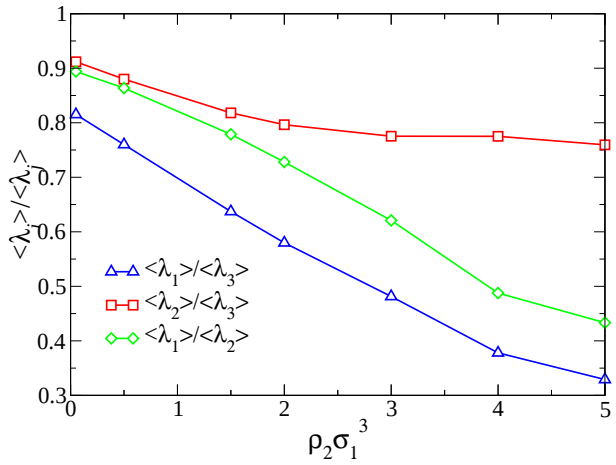

FIG. S4: Ratios of the eigenvalues of the inertia tensor for $f_1 = 263$, $f_2 = 64$, $\rho_1\sigma_1^3 = 0.345$, and $\delta = 0.4$.

Table SII reports the absolute value of the eigenvalues. This is found to genuinely decrease as the cage shrinks, even taking into account the drop related to the decrease in the average number of nearest neighbors, N_{11}.

- *Comparison with binary mixtures of hard spheres with* $\delta = 0.4$ *and* $\delta = 0.5$.

  To provide evidence that the asymmetric glass reported for a binary mixture of star polymers is a unique feature of soft interactions, we have performed event driven simulations of hard sphere mixtures with size ratio $\delta = 0.4$ and $\delta = 0.5$, at $\rho_1\sigma_1^3 = 0.993$, a value correspondingly close to the hard-sphere glass transition density. The mass ratio of the particles is assumed to scale as δ^3, proportional to the relative volume of the colloids. As shown in Fig. S5(a), for $\delta = 0.4$ we observe only a slowing down of the dynamics upon increasing the density of smaller spheres, confirming the absence of reentrance at this size ratio.

$\rho_2\sigma_1^3$	N_{11}	$\langle\lambda_1\rangle/(N_{11}\sigma_1^2)$	$\langle\lambda_2\rangle/(N_{11}\sigma_1^2)$	$\langle\lambda_3\rangle/(N_{11}\sigma_1^2)$	k_2
0.05	12.5	1.55	1.74	1.90	0.0101
0.5	10.0	1.32	1.53	1.74	0.0184
1.5	6.54	1.02	1.31	1.61	0.0486
2.0	5.63	0.866	1.19	1.49	0.0711
3.0	4.25	0.670	1.08	1.39	0.123
4.0	3.34	0.472	0.969	1.25	0.207
5.0	2.88	0.348	0.819	1.06	0.261
fcc	12	1.71	1.71	1.71	0

TABLE SII: Number of nearest neighbors, (normalized) eigenvalues of the inertia tensor and anisotropy parameter as a function of the density of small stars for $\delta = 0.4$. As a comparison, we also quote the corresponding values for a fcc lattice at the same $\rho_1\sigma_1^3 = 0.345$.

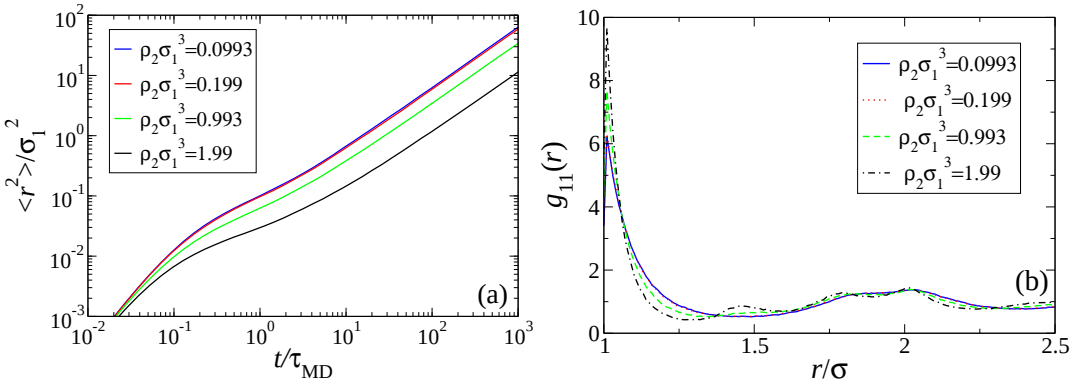

FIG. S5: Dynamical and structural properties of hard sphere mixtures from simulations. (a) Mean squared displacement of large hard-spheres with increasing additive density at $\rho_1\sigma_1^3 = 0.993$ and $\delta = 0.4$. (b) $g_{11}(r)$ of large hard spheres in the binary hard sphere mixture with $\delta = 0.4$.

Concerning the evolution of the structure, we see in Fig. S5(b) the emergence of several small peaks in $g_{11}(r)$, corresponding to a layering of small spheres around the large ones. Of course, the hard-core prevents any progressive shift in the location of the main peak. The first minimum moves slightly, giving rise to a moderate decrease of the number of nearest neighbors. More interestingly, Fig. 4(d) of the manuscript shows that the anisotropy

parameter k_2 grows only from 0.012 to 0.019 for $\delta = 0.4$ and to 0.025 for $\delta = 0.5$, indicating that a rather spherical shape of the cages is retained for all studied ρ_2. Despite the fact that large ρ_2 values are difficult to simulate, the absence of any significant trend is sufficient to affirm that no asymmetric glass is expected in hard colloids.

---

[1] Roovers, J.,Zhou, L., Toporowski, P. W., van der Zwan, M. Iatrou, H. & Hadjichristidis, N. Regular star polymers with 64 and 128 arms — models for polymeric micelles. *Macromolecules* **26**, 4324–4331 (1993).

[2] Zaccarelli, E., Mayer, C., Asteriadi, A., Likos, C.. N., Sciortino, F., Roovers, J., Iatrou, H., Hadjichristidis, N., Tartaglia, P., Löwen, H. & Vlassopoulos, D. Tailoring the Flow of Soft Glasses by Soft Additives. *Phys. Rev. Lett.* **95**, 268301 (2005).

[3] Munam, A. Ph.D. thesis, University of Waterloo (2007).

[4] Teertstra, S. J. & Gauthier, M. Viscoelastic Properties of Arborescent Polystyrene-*graft*-polyisoprene Copolymers. *Macromolecules* **40**, 1657–1666 (2007).

[5] Laurati, M., Stellbrink, J., Lund, R., Willner, L., Richter, D. & Zaccarelli, E. Starlike Micelles with Starlike Interactions: A Quantitative Evaluation of Structure Factors and Phase Diagram. *Phys. Rev. Lett.* **94**, 195504 (2005).

[6] Ozon, F., Petekidis, G. & Vlassopoulos, D. Signatures of nonergodicity transition in a soft colloidal system. *Ind. Eng. Chem. Res.* **45**, 6946–6952 (2006).

[7] von Ferber, C., Jusufi, A., Watzlawek, M., Likos, C. N. & Löwen, H. Polydisperse star polymer solutions. *Phys. Rev. E* **62**, 6949–6956 (2000).

[8] Foffi, G., Sciortino, F., Tartaglia, P., Zaccarelli, E., Lo Verso, F., Reatto, L., Dawson, K. & Likos, C. N. Structural Arrest in Dense Star-Polymer Solutions. *Phys. Rev. Lett.* **90**, 238301 (2003).

[9] Barrat, J.-L. & Latz, A. Mode coupling theory for the glass transition in a simple binary mixture. *J. Phys.: Condens. Matter* **2**, 4289–4295 (1990).

[10] Götze, W. in *Amorphous and Liquid Materials*, p. 34, Vol. 118 of *NATO Advanced Study Institute, Series E: Applied Sciences*, edited by E. Lüscher, G. Fritsch, G. Jacucci (Nijhoff, Dordrecht, 1987).

[11] Hansen, J.-P. & McDonald, I. R. *Theory of Simple Liquids* (Academic, London, ed. 3, 2006).

[12] Rogers, F. J. & Young, D. A., *Phys. Rev. A* **30**, 999–1007 (1984).

[13] Nägele, G. & Bergenholtz, J. Linear viscoelasticity of colloidal mixtures. *J. Chem. Phys.* **108**, 9893–9904 (1998).

[14] Grest, G. S., Fetters, L. J., Huang, J. S. & Richter, D. Star Polymers: Experiment, Theory, and Simulation. *Adv. Chem. Phys.* **XCIV**, 67 (1996).

[15] Goldstein, H. *Classical Mechanics* (Addison-Wesley, Reading, ed. 2, 1980).